ISSN: 2688-8645

The Study on the Multi-Factor Influences on Hydraulic Fracturing Expansion Based on Numerical Simulation

Zhiyu Zhou, Hongyong Guo

College of Petroleum Engineering, Xi'an Shiyou University, Xi'an, Shaanxi 710065, China

Abstract

With the development of unconventional oil and gas resources, hydraulic fracturing technology has played a crucial role in the exploitation of shale gas, tight oil, and other reservoirs. The expansion morphology of fractures significantly impacts the fracturing effectiveness, and the geometric characteristics of the fractures are influenced by rock mechanical parameters and geological conditions. This study systematically investigates the effects of Young's modulus, Poisson's ratio, brittleness index, and horizontal stress difference on the fracture propagation path, width, and length in hydraulic fracturing, using numerical simulation methods. The simulation results indicate that Young's modulus is closely related to fracture stiffness, with higher values leading to reduced fracture width and increased length. Poisson's ratio affects the deformation behavior of fractures, with larger Poisson's ratios causing more uniform fracture deformation. When the brittleness index is higher, fractures tend to adopt a more elongated shape. The horizontal stress difference influences the directional propagation of fractures, with larger stress differences resulting in more linear fracture shapes. This study provides theoretical support for fracture design and fracturing parameter optimization in hydraulic fracturing operations, aiming to improve fracturing efficiency and optimize oil and gas recovery.

Keywords

Hydraulic Fracturing; Fracture Propagation; Young's Modulus; Poisson's Ratio; Brittleness Index; Horizontal Stress Difference; Numerical Simulation.

1. Introduction

As global energy demand continues to grow and traditional oil and gas resources gradually deplete, the development of unconventional energy sources has become an important component of global energy strategy. Unconventional resources such as shale gas and tight oil, with their vast potential, have attracted widespread attention from the oil exploration and production industries worldwide. Hydraulic fracturing, as a mature extraction technology, has played a key role in the development of shale gas and tight oil. This technology involves injecting high-pressure fluids into underground rock formations to induce the formation and propagation of fractures, thereby significantly enhancing the permeability of reservoirs and enabling the effective extraction of previously inaccessible oil and gas resources.

The research methods for hydraulic fracturing mainly include experimental studies(Z.-L. Zhou et al., 2024) and numerical simulation studies(Ismail & Azadbakht, 2024). Numerical simulations have rapidly developed due to their advantages such as low cost, no need for field experiments, and the ability to handle complex geological conditions. Currently, commonly used numerical simulation methods include Cohesive Zone Model(Chen et al., 2016; Guo et al., 2017), DDA (Choo et al., 2016; Hu et al., 2021), XFEM (Chen et al., 2023; Dong et al., 2021; Zhou et al., 2025), DEM(Huang et al., 2023; Li et al., 2022), FEM(Liao et al., 2020; Zhang et al., 2024),

ISSN: 2688-8645

and Phase Field Method(Gong et al., 2025; Ni et al., 2020). These methods have made significant progress in the field of hydraulic fracturing.

Among them, the Cohesive Zone Model (CZM) is one of the effective alternative methods for describing fracture propagation(Li et al., 2023). This model assumes the presence of a process zone at the crack tip and uses a traction-separation (T-S) constitutive model to describe the fracture behavior within this process zone, thus avoiding the stress singularity problem at the crack tip in linear elastic fracture mechanics. This makes CZM more stable when simulating fracture propagation and rupture processes.

Sun et al. (2012) conducted a study on hydraulic fracture propagation in oil shale using cohesive elements. They found that fractures are elliptical in shape and influenced by the anisotropic properties of oil shale and in-situ stresses, with fracture propagation varying in different directions. As fracturing fluid is injected, the fracture width increases, and stress concentrates at the fracture tip, ultimately promoting fracture extension. The study also examined the initiation and propagation of fractures in horizontal wells in oil shale, analyzing the effects of geological and engineering factors on fracture morphology. Chen et al. (2023). used extended finite element methods to simulate the effects of factors such as Poisson's ratio and brittleness index on fracture width and length, and explored how completion hole angle, fracturing fluid viscosity, and injection rate affect fracture propagation. The results indicated that Young's modulus influences fracture length and width, while the brittleness index also alters fracture morphology. Li et al. (2019) used extended finite element methods (XFEM) to establish a coupled flow-stress model, simulating fracture deflection behavior and experimentally validating the model's accuracy. The study found that lower stress differences, larger perforation angles, and deeper perforations lead to larger fracture deflection angles, and increasing injection rate and fluid viscosity significantly enhance fracture deflection. X. Zhou et al. (2024) studied the influencing factors of three-dimensional multi-cluster hydraulic fracturing, using finite element methods to simulate the effects of cluster spacing, Young's modulus, Poisson's ratio, and other parameters on fracture propagation. The results showed that larger cluster spacing reduces interaction between fractures, while more clusters increase mutual influence; an increase in Young's modulus leads to a decrease in fracture width and height but an increase in length. Liu et al. (2022) investigated hydraulic fracture propagation in natural fracture networks, using cohesive elements to simulate propagation and analyzing the influence of in-situ horizontal stress, rock tensile strength, and natural fracture cementing strength. The study concluded that when horizontal stress differences are small, hydraulic fractures tend to propagate along natural fractures, forming a more complex fracture network, but as the stress difference increases, fractures become more linear and the influence of natural fractures diminishes. Zhang et al. (2023) simulated fracture propagation under different fracturing schemes, finding that simultaneous and sequential fracturing increase stress interference between fractures, limiting fracture propagation, while zipper fracturing reduces stress interference and promotes fracture extension. Multi-cluster fracturing limits fracture propagation due to strong interference between fractures. Guipu et al. (2024) developed a fluid-structure coupling model to simulate multi-fracture propagation, analyzing how perforation parameters (such as diameter, depth, density, and phase angle) affect fracture initiation pressure. The study found that higher perforation density significantly reduces initiation pressure, while increasing perforation diameter and depth further lowers initiation pressure. Additionally, horizontal stress difference, rock tensile strength, natural fracture dip, and complex fracture networks also significantly impact hydraulic fracture propagation(Chen et al., 2025; Hu et al., 2025; Zhang et al., 2025).

In this study, considering the influence of rock mechanical parameters (such as Young's modulus, Poisson's ratio, and brittleness index) and geological factors (such as horizontal stress difference) on fracture propagation morphology, numerical simulations will be conducted to

ISSN: 2688-8645

analyze the effects of these factors on fracture propagation path, width, length, and other aspects. Through systematic numerical simulations, this research aims to provide a theoretical basis for fracture design and parameter optimization in hydraulic fracturing operations, thereby helping to improve fracturing effectiveness and achieve more efficient oil and gas recovery.

2. Methodology

2.1. The Fluid-Solid Coupling Governing Equations in the Fracturing Process

The concept of effective stress was first introduced in the 1920s and has been applied in practical engineering studies, verifying its applicability. For porous media, when the pores are filled with fluid, the fluid applies a normal pressure on the rock framework, which is isotropic and referred to as pore pressure. In addition to the fluid pressure, the stress transmitted between the rock skeleton is defined as the effective stress σ. When the boundaries of the porous media are subjected to external loads, the solid skeleton deforms, and effective stress is generated at the contact surface. According to Biot's law, the relationship between effective stress and total stress in saturated porous media is given as follows:

$$\sigma = \bar{\sigma} + \delta\alpha p_w \tag{1}$$

In the above equation, σ is the total stress applied to the porous medium, $\bar{\sigma}$ is the effective stress acting on the porous medium , δ is the Kronecker constant. α is the Biot effective stress coefficient, and p_w is the pore pressure around the fractures.

The equilibrium equation of the matrix in the hydraulic fracturing process is given by(Sigrist, 2015):

$$\int_V (\bar{\sigma} + \delta p_w)\delta_\varepsilon \, dV = \int_S a \cdot \delta_v dS + \int_V b \cdot \delta_v dV \tag{2}$$

where δ_ε is the virtual strain rate, a is the surface force vector per unit area, δ_v is the virtual velocity field, dV is the unit volume, and dS represents the unit surface area on which the surface forces act.

And the fluid flow satisfies the mass balance equation(Guo et al., 2017):

$$\frac{\partial(P_w\varphi)}{\partial t} + \nabla \cdot (P_w \varphi v_w) = 0 \tag{3}$$

According to Darcy's law, the relationship between the flow velocity of the fracturing fluid in the pores and the pore pressure gradient is given by(Li & Ghosh, 2006):

$$v_w = -\frac{1}{\rho_w g n_w} k \cdot \left(\frac{\partial p_w}{\partial x} - g\rho_w\right) \tag{4}$$

where k is the matrix permeability, and g is the gravitational acceleration, ρ_w represents the density of the injected fluid;v_w is the fluid seepage velocity; φ represents the dimensionless dynamic porosity of the reservoir.

2.2. The Viscoelastic Damage Element Model for Crack Propagation.

The initiation of rock fracture is described using the viscoelastic band and traction-separation criterion. Prior to the initial damage, a linear elastic model with a diagonal stiffness matrix is used(Bastola & Chugh, 2015).

$$\bar{t} = \begin{Bmatrix} t_n \\ t_s \\ t_t \end{Bmatrix} = K\delta = \begin{Bmatrix} k_{nn} & 0 & 0 \\ 0 & k_{ss} & 0 \\ 0 & 0 & k_{tt} \end{Bmatrix} = \begin{Bmatrix} \delta_n \\ \delta_s \\ \delta_t \end{Bmatrix} \tag{5}$$

ISSN: 2688-8645

in the equation, $\bar{t}$ is the stress vector applied to the Cohesive bonding element; t_n, t_s, and t_t are the stresses in the normal direction (perpendicular to the surfaces of the Cohesive element), the first tangential direction, and the second tangential direction, respectively; K is the elastic stiffness matrix of the Cohesive element.

This study uses the maximum principal stress criterion to determine whether the cohesive element undergoes initial damage. Specifically, when the ratio of the stress value in any direction of the three-dimensional stress to its corresponding critical value exceeds 1, hydraulic fracturing begins. The formula is as follows(Bajpai & Singh, 2013):

$$\max\left\{\frac{\langle t_n\rangle}{t_n^0}, \frac{t_s}{t_s^0}, \frac{t_t}{t_t^0}\right\} = 1 \tag{6}$$

after damage occurs, the damage evolution criterion based on the maximum fracture displacement is used to describe the degradation of material stiffness. The unit damage is determined by comparing and evaluating the effective displacement with the critical displacement value.

$$\delta_m = \sqrt{\langle t_n\rangle^2 + {t_s}^2 + {t_t}^2} \tag{7}$$

The fracture propagation process is described using the stiffness degradation of the viscoelastic elements, and its expression is given by(Zhu et al., 2015):

$$\begin{aligned} t_n &= \begin{cases} (1-D)T_n & (T_n \geq 0) \\ T_n & (T_n < 0) \end{cases} \\ t_s &= (1-D)T_s \\ t_t &= (1-D)T_t \end{aligned} \tag{8}$$

D represents the overall damage degree of the cohesive element, which increases linearly from 0 to 1 after the initiation of element damage. The corresponding expression is given by(Turon et al., 2006):

$$D = \frac{d_m^f(d_m^{\max} - d_m^0)}{d_m^{\max}\left(d_m^f - d_m^0\right)} \tag{9}$$

here, t_n^0, t_s^0, and t_t^0 represent the critical normal stress and the critical shear stresses in the two directions when the cohesive element fails. T_s and $T_n$are the normal stress components before damage, and T_t is the shear stress component before damage. $d_m^{\max}$ is the maximum displacement amplitude reached by the element during the loading process; d_m^f is the displacement amplitude when the element is fully damaged; d_m^0 is the displacement amplitude when the element experiences initial damage.

3. Model Verification

To validate the accuracy of the model, this study uses the analytical solution of the KGD model(Detournay, 2004) to verify the simulation results. This solution is used to describe the width and length of hydraulic fractures in impermeable media. Based on the symmetry of the KGD model, half of the model is selected for analysis. The model dimensions and boundary conditions are shown in the Fig 1 It is assumed that an incompressible Newtonian fluid is injected at a constant rate. Fig 2 compares the analytical solution with the numerical solution, and it can be seen that the analytical solution closely matches the numerical solution, indicating that the proposed model effectively simulates the hydraulic fracturing process.

ISSN: 2688-8645

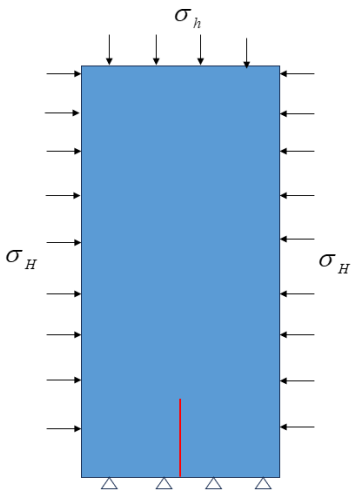

Fig 1. Schematic of the verification model

When setting the boundary conditions, the displacement in the X-direction is set to 0, the upper boundary displacement in the Y-direction is set to 0, and the lower boundary is set as a symmetric boundary. The magnitudes of the maximum and minimum horizontal stresses are equal.

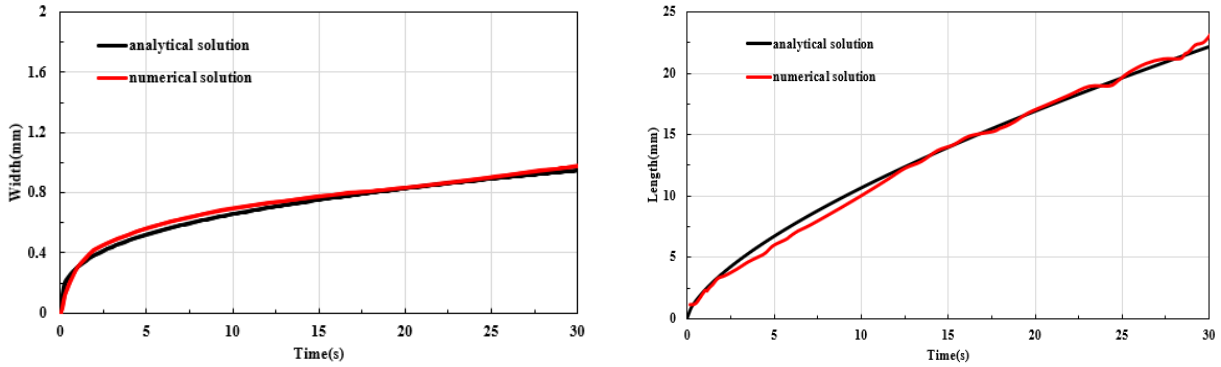

(a) Fracture width (b) Fracture length

Fig 2. Comparison of numerical solution and analytical solution.

4. Nature Fracture Modeling

Based on the finite element method, a two-dimensional fluid-structure coupling model was established to study the impact of pre-set natural fracture clusters with specified angles on hydraulic fracturing propagation. To simplify the model and accelerate the computation, a one-sided fracture propagation path was designed, with the model size set to 50m × 50m. The matrix rock body uses two-dimensional four-node bilinear displacement-pore pressure elements (CPE4P), and the fracture propagation path employs six-node displacement-pore pressure cohesive elements (COH2D4P). To ensure the accuracy of the numerical simulation, the boundary conditions of the model were set as follows: displacement constraints in the X-direction were applied to the left and right boundaries, while displacement constraints in the Y-direction were applied to the upper and lower boundaries, with constant pore pressure boundary conditions. To improve the convergence of the simulation process, the injection rate was linearly increased over 10 seconds, ensuring a smooth transition of pressure application and the stability of the simulation results. Fig 3 shows the generation process of the random fracture network, along with the model's dimensions and injection point location, and Table 1 lists the basic input parameters of the model.

ISSN: 2688-8645

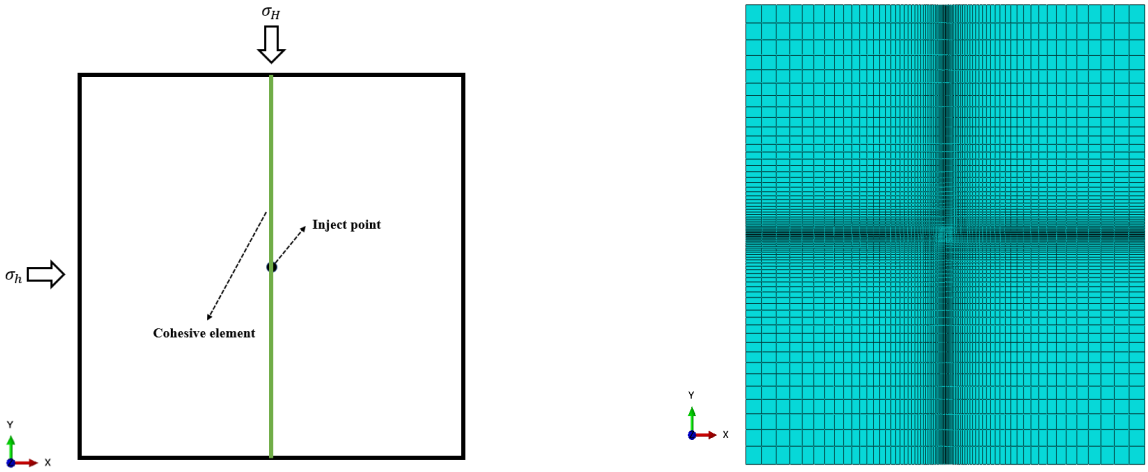

(a)Schematic of the model (b)Mesh discretization

Fig 3. Schematic of the two-dimensional geometric model.

Table 1. Model Parameters

Parameters	Value	Parameters	Value
Young's modulus (GPa)	15	Porosity	0.1
Poisson's ratio	0.25	Permeability (mD)	1
Tensile strength of rock (MPa)	6	Leak-off coefficient $m/(Pa \cdot s)$	1×10^{-14}
Minimum horizontal stress (MPa)	30	Injection rate (m^2/s)	0.001
Maximum horizontal stress (MPa)	40	Fluid viscosity ($Pa \cdot s$)	0.001
Vertical stress (MPa)	25	Pore pressure (MPa)	20

In the simulation process, by analyzing the relationship between fracture width, length, and geological and engineering parameters (such as Young's modulus, Poisson's ratio, and brittleness index), the direction and morphology of fracture propagation can be tracked in real-time. Fig 4 shows the fracture propagation path extracted from the simulation results. The fracture length and width data in the subsequent analysis are derived from this path.

Fig 4. Extract the path.

5. Simulation Results and Discussion

5.1. The Effect of Young's Modulus

The Young's modulus (E) of rocks is a key parameter characterizing their basic mechanical properties and an important basis for designing reservoir fracturing schemes. Its value reflects the ease with which rocks deform under external loads. In this study, we assume that the initial

ISSN: 2688-8645

fracture direction aligns with the direction of the maximum horizontal principal stress. Using the parameters shown in Table 1 as the basis for simulation, the effect of varying the Young's modulus (set to 15 GPa, 20 GPa,and 30 GPa, respectively) on fracture morphology is analyzed.

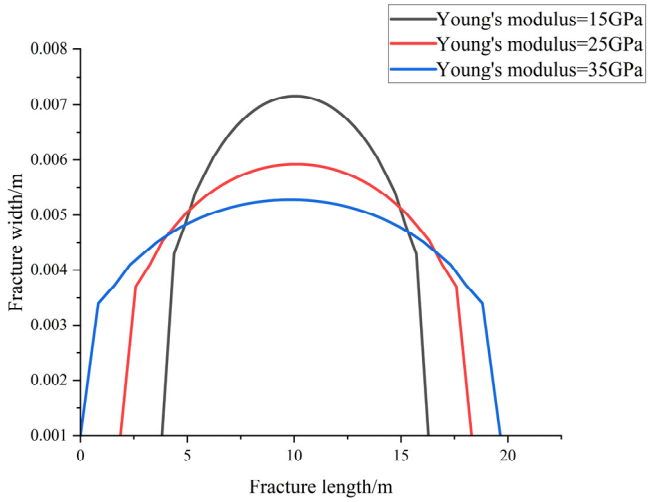

Fig 5. Relationship between fracture width and length under different Young's moduli.

As shown in Fig 5, keeping the injection regime and boundary conditions unchanged and only varying the matrix's Young's modulus, show that the width distribution along the fracture length peaks at the center and is approximately symmetric around the fracture center. As E increases, the peak width decreases monotonically, and the effective fracture length increases monotonically. From the data, at $E = 15\ GPa$, the peak width is approximately 7.1 mm, at $E = 25\ GPa$ it is about 6 mm (a reduction of about 16% from the former), and at $E = 35\ GPa$ it is about 5 mm (a further reduction of 17% from 25 GPa, a total reduction of 30% from 15 GPa). The corresponding effective fracture lengths increase from about 12 m to 17 m and 20 m (a total increase of 67% compared to 15 GPa). This trend suggests that rocks with lower Young's modulus tend to form "short and wide" fractures, while those with higher Young's modulus tend to form "long and narrow" fractures. These results indicate that the fracture morphology is not only controlled by the Young's modulus but also reflects the influence of rock stiffness on the fracture propagation direction. Therefore, in hydraulic fracturing operations, considering the variations in rock stiffness, the size of proppant grains and sand carrying capacity should be optimized based on regions with different Young's moduli to ensure stable fracture propagation and maximize the fracture coverage.

5.2. The Effect of Poisson's Ratio

Poisson's ratio (v), as a reference parameter for rock brittleness, is used to study and analyze the influence of Poisson's ratio on fracture morphology. Using the base data from Table 1, the Poisson's ratio in the reservoir is varied to values of 0.15, 0.25, and 0.35.

In Fig 6, the relationship between fracture width and length under different Poisson's ratios is shown. The figure illustrates that as the Poisson's ratio increases, the fracture width remains relatively consistent and reaches its peak in the middle of the fracture length. This suggests that, under different Poisson's ratios, the fracture expansion pattern and distribution do not show significant differences. Specifically, when the Poisson's ratio is 0.15, the fracture width is slightly larger, especially at the two ends of the fracture. As the Poisson's ratio increases to 0.25 and 0.35, the fracture width gradually decreases, and as the fracture length increases, the width becomes more stable, with the fracture expansion becoming more uniform. This may indicate that, at higher Poisson's ratios, the rock deforms more uniformly and elastically, enhancing the stability of the fracture and making it easier to maintain a more uniform fracture width. This trend also suggests that under high Poisson's ratio conditions, the fracture expansion is

ISSN: 2688-8645

smoother, the width variation between fractures is smaller, and the fracture shape tends to be more symmetric and uniform, which could be a positive factor for the controllability of hydraulic fracturing operations.

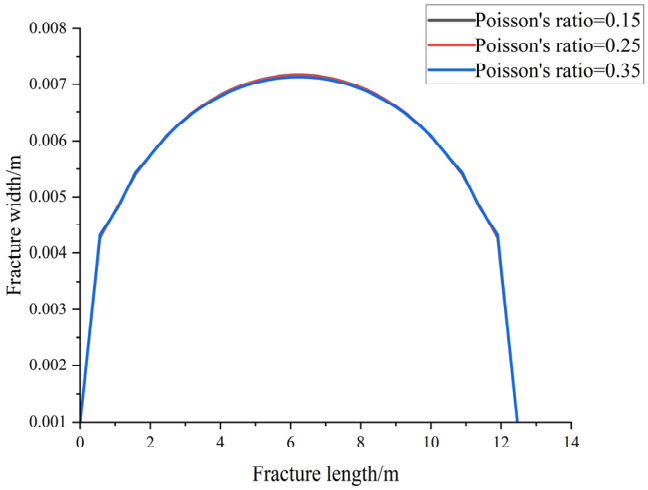

Fig 6. The relationship between fracture width and length under different Poisson's ratios.

5.3. The Effect of Brittleness Index

The brittleness of rocks reflects their ability to resist large deformations under external loads before failure, indicating that they absorb less energy before breaking and do not undergo significant plastic deformation during this process. The brittleness index quantifies the brittle characteristics of rocks. Successful fracturing experiences in North American shale suggest that the higher the brittleness index, the better the shale's compressibility and the more effective the hydraulic fracturing. However, the methods for calculating the brittleness index of rocks in strata vary across different regions, leading to differences in the values obtained. Rickman et al. (2008)proposed that the brittleness index could be calculated by altering the rock's Young's modulus and Poisson's ratio. The brittleness index derived using this method was then applied in numerical simulations, with the specific parameters for calculating the brittleness index shown in Table 1.

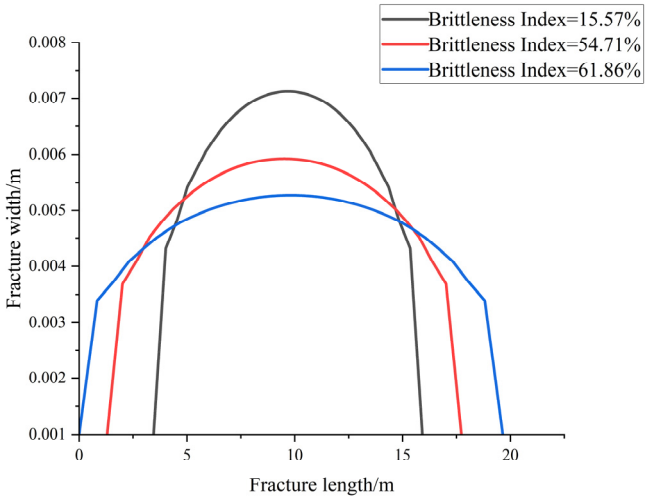

Fig 7. The relationship between fracture width and length under different brittleness indices.

According to the simulation results shown in Fig 7, the brittleness index, as a combined indicator of Young's modulus and Poisson's ratio, has a significant impact on the fracture width distribution in hydraulic fracturing. The figure illustrates the relationship between fracture width and length under different brittleness indices. As the brittleness index increases, the peak fracture width gradually decreases. Specifically, at a brittleness index of 15.57%, the fracture

ISSN: 2688-8645

width is relatively large, especially in the middle of the fracture; whereas at brittleness indices of 54.71% and 61.86%, the fracture width gradually narrows, and the fracture expansion becomes more uniform. From the figure, it can be seen that rocks with a high brittleness index tend to form narrower and longer fractures, while rocks with a low brittleness index tend to form wider and shorter fractures. This trend indicates that rocks with a higher brittleness index are more likely to generate long and narrow fractures in hydraulic fracturing, while rocks with a lower brittleness index tend to form wider and shorter fractures. Therefore, rocks with higher brittleness have a stronger hydraulic fracturing response, allowing for effective fracture propagation and improving the connectivity of the fracture network. This has important guiding significance for proppant selection, fracture design, and fracturing efficiency in hydraulic fracturing operations.

5.4. The Effect of Horizontal Stress Difference

Horizontal stress difference is one of the key factors influencing fracture propagation. To investigate the effect of horizontal stress difference on fracture width, this study maintains the basic data as shown in Table 1, while varying the horizontal stress difference (ΔS), setting it to 0 MPa, 6 MPa, and 14 MPa, respectively. This variation helps to analyze the change patterns of fracture width under different horizontal stress difference conditions and their impact on hydraulic fracturing efficiency. By comparing fracture development under different stress difference conditions, the mechanism of stress difference influencing fracture extension path and width can be revealed, providing theoretical support for optimizing hydraulic fracturing design.

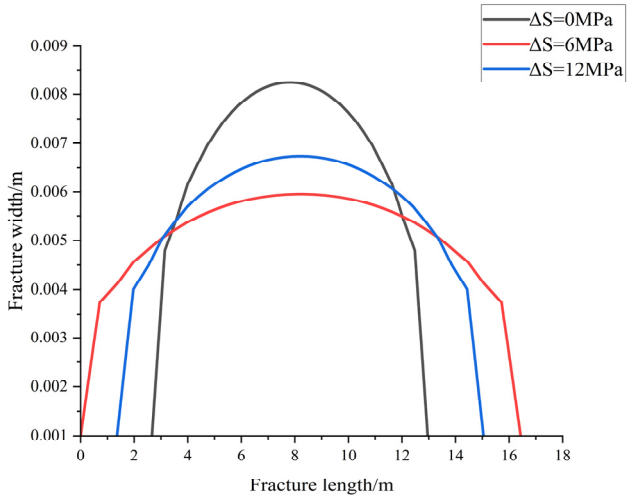

Fig 8. The relationship between fracture width and length under different horizontal stress differences

As shown in the figure, with the increase of the horizontal stress difference (ΔS), both the fracture width and length undergo significant changes. When ΔS = 0 MPa, the fracture width is at its maximum, about 0.007 m, and the fracture length reaches approximately 18 m, presenting a relatively uniform expansion pattern. As the horizontal stress difference increases to 6 MPa, the fracture width decreases to about 0.0065 m, a reduction of approximately 7.1% compared to $\Delta S = 0\ MPa$. The fracture expansion speed and pattern change, becoming more elongated, and the fracture length shortens to about 14 m, a reduction of about 22.2%. When the horizontal stress difference further increases to 12 MPa, the fracture width decreases to about 0.004 m, a 42.9% reduction compared to $\Delta S = 0\ MPa$. The fracture length also shortens to 12 m, a 33.3% reduction. This indicates that a higher horizontal stress difference significantly inhibits the fracture expansion, reducing both the fracture width and length, and the fractures exhibit a more elongated shape. This trend suggests that a larger stress difference will limit

ISSN: 2688-8645

fracture expansion, hindering the formation of fracture networks. It highlights the importance of considering the impact of stress difference on fracture morphology in actual hydraulic fracturing operations.

6. Conclusion

1.As the Young's modulus increases, the fracture width gradually decreases, and the fracture length increases. Low Young's modulus regions are more likely to form "short and wide" fractures, while high Young's modulus regions tend to form "long and narrow" fractures. This indicates that higher Young's modulus results in more stable fracture propagation and makes the fracture morphology more uniform.

2.The increase in Poisson's ratio leads to a decrease in fracture width, and the fracture propagation becomes more symmetrical. Lower Poisson's ratio makes fractures more likely to propagate and form wider fractures, while higher Poisson's ratio results in more uniform fracture propagation, and the fractures are narrower, indicating that rocks with higher Poisson's ratio have stronger deformation ability and higher fracture stability.

3.The higher the brittleness index, the stronger the rock's brittleness. After hydraulic fracturing, the fracture width is smaller, and the fracture length increases. Simulation results show that as the brittleness index increases, the fracture propagation becomes more uniform and stable, suggesting that high brittleness rocks are more likely to form longer fractures during hydraulic fracturing.

4.With the increase of horizontal stress difference, the fracture width gradually decreases, especially at the fracture front. When the horizontal stress difference reaches 6 MPa, the fracture propagation is significantly affected, and the fracture width may decrease by about 30%. However, the effect of horizontal stress difference on fracture width is relatively limited, mainly reflected in the fracture propagation path and length. Under larger stress differences, the fracture length increases significantly, while the change in fracture width is relatively small. This indicates that horizontal stress difference has an important impact on the geometric morphology of fractures, especially in terms of fracture propagation direction and stability.

References

[1] Bajpai, V., & Singh, R. (2013, 2013/01/01/). Brittle damage and interlaminar decohesion in orthogonal micromachining of pyrolytic carbon. International Journal of Machine Tools and Manufacture, 64, 20-30. https://doi.org/10.1016/j.ijmachtools.2012.07.007.

[2] Bastola, S., & Chugh, Y. P. (2015). Shear Strength and Stiffness of Bedding Planes and Discontinuities in the Immediate Roof Rocks Overlying the No 6 Coal Seam in Illinois. 13th ISRM International Congress of Rock Mechanics.

[3] Chen, B., Li, S., & Tang, D. (2025, 2025/04/15/). Numerical simulation study on hydraulic fracture propagation of multi-cluster fracturing of horizontal well in deep fractured coal seams. Engineering Fracture Mechanics, 318, 110983. https://doi.org/10.1016/j.engfracmech.2025.110983.

[4] Chen, H., Wei, C., Lou, X., Song, H., Pan, Y., Yang, P., Guan, J., & Wang, S. (2023, 2023/07/01). Numerical Simulation of Fracture Initiation and Propagation in Oil Shale Horizontal Wells. Chemistry and Technology of Fuels and Oils, 59(3), 534-550. https://doi.org/10.1007/s10553-023-01554-0.

[5] Chen, Z., Jeffrey, R. G., Zhang, X., & Kear, J. (2016). Finite-Element Simulation of a Hydraulic Fracture Interacting With a Natural Fracture. SPE Journal, 22(01), 219-234. https://doi.org/10. 2118 /176970-pa.

[6] Choo, L. Q., Zhao, Z., Chen, H., & Tian, Q. (2016, 2016/06/01/). Hydraulic fracturing modeling using the discontinuous deformation analysis (DDA) method. Computers and Geotechnics, 76, 12-22. https://doi.org/10.1016/j.compgeo.2016.02.011.

[7] Detournay, E. (2004). Propagation Regimes of Fluid-Driven Fractures in Impermeable Rocks. International Journal of Geomechanics, 4(1), 35-45. https://doi.org/10.1061/(ASCE)1532-3641 (2004) 4:1(35).

[8] Dong, Y., Tian, W., Li, P., Zeng, B., & Lu, D. (2021, 2021/12/01/). Numerical investigation of complex hydraulic fracture network in naturally fractured reservoirs based on the XFEM. Journal of Natural Gas Science and Engineering, 96, 104272. https://doi.org/10.1016/j.jngse.2021.104272.

[9] Gong, X., Jin, Z., Ma, X., Liu, Y., Li, G., & Bian, Y. (2025, 2025/03/01). Simulation Investigation of Hydraulic Fracture Propagation Patterns at Lithological Interfaces Based on the Phase-Field Method. Rock Mechanics and Rock Engineering, 58(3), 2803-2828. https://doi.org/10. 1007/ s00603-024-04258-x.

[10] Guipu, J., Hui, Z., Bin, F., & Shuo, H. (2024, 2024/09/01). Influence of Perforation on Fracture Initiation in Horizontal Wells and Parameter Optimization. Chemistry and Technology of Fuels and Oils, 60(4), 910-919. https://doi.org/10.1007/s10553-024-01753-3.

[11] Guo, J., Luo, B., Lu, C., Lai, J., & Ren, J. (2017, 2017/12/01/). Numerical investigation of hydraulic fracture propagation in a layered reservoir using the cohesive zone method. Engineering Fracture Mechanics, 186, 195-207. https://doi.org/10.1016/j.engfracmech.2017.10.013.

[12] Hu, Y., Li, X., Zhang, Z., He, J., & Li, G. (2021). Numerical modeling of complex hydraulic fracture networks based on the discontinuous deformation analysis (DDA) method. Energy Exploration & Exploitation, 39(5), 1640-1665. https://doi.org/10.1177/0144598720981532.

[13] Hu, Y., Wang, Y., Wang, Q., Zhao, J., Zhu, J., Li, X., & Yang, Y. (2025). The propagation laws of hydraulic fractures under the influence of natural fracture zones. Physics of fluids, 37(1). https:// doi. org/10.1063/5.0244800.

[14] Huang, L., He, R., Yang, Z., Tan, P., Chen, W., Li, X., & Cao, A. (2023, 2023/02/01/). Exploring hydraulic fracture behavior in glutenite formation with strong heterogeneity and variable lithology based on DEM simulation. Engineering Fracture Mechanics, 278, 109020. https://doi. org/10. 1016/j.engfracmech.2022.109020.

[15] Ismail, A., & Azadbakht, S. (2024). A comprehensive review of numerical simulation methods for hydraulic fracturing. International Journal for Numerical and Analytical Methods in Geomechanics, 48(5), 1433-1459. https://doi.org/10.1002/nag.3689.

[16] Li, J., Dong, S., Hua, W., Yang, Y., & Li, X. (2019). Numerical Simulation on Deflecting Hydraulic Fracture with Refracturing Using Extended Finite Element Method. Energies, 12(11), 2044. https:// www.mdpi.com/1996-1073/12/11/2044.

[17] Li, M., Wu, J., Li, J., Zhuang, L., Wang, S., & Zhang, F. (2022, 2022/11/01/). Modeling of hydraulic fracturing in polymineralic rock with a grain-based DEM coupled with a pore network model. Engineering Fracture Mechanics, 275, 108801. https://doi.org/10.1016/j. engfracmech. 2022. 108801.

[18] Li, S., & Ghosh, S. (2006, 2006/10/01). Multiple cohesive crack growth in brittle materials by the extended Voronoi cell finite element model. International Journal of Fracture, 141(3), 373-393. https: //doi.org/10.1007/s10704-006-9000-2.

[19] Li, X. J., Zhao, H. F., Xu, K. Q., He, Y. L., Wang, C. W., & Yao, W. J. (2023, 2023/01/01). A review on the application of cohesive zone model in hydraulic fracturing. IOP Conference Series: Earth and Environmental Science, 1124(1), 012073. https://doi.org/10.1088/1755-1315/1124/1/012073.

[20] Liao, J., Gou, Y., Feng, W., Mehmood, F., Xie, Y., & Hou, Z. (2020, 2020/02/01). Development of a full 3D numerical model to investigate the hydraulic fracture propagation under the impact of orthogonal natural fractures. Acta Geotechnica, 15(2), 279-295. https://doi.org/10.1007/s11440-019-00862-2.

[21] Liu, Y., Hu, Y., & Kang, Y. (2022). The Propagation of Hydraulic Fractures in a Natural Fracture Network: A Numerical Study and Its Implications. Applied Sciences, 12(9), 4738. https://doi.org/ 10. 3390/app12094738.

ISSN: 2688-8645

[22] Ni, L., Zhang, X., Zou, L., & Huang, J. (2020, 2020/10/01). Phase-field modeling of hydraulic fracture network propagation in poroelastic rocks. Computational Geosciences, 24(5), 1767-1782. https://doi.org/10.1007/s10596-020-09955-4.

[23] Rickman, R., Mullen, M., Petre, E., Grieser, B., & Kundert, D. (2008). A Practical Use of Shale Petrophysics for Stimulation Design Optimization: All Shale Plays Are Not Clones of the Barnett Shale SPE Annual Technical Conference and Exhibition. https://doi.org/10.2118/115258-MS.

[24] Sigrist, J.-F. (2015, 10/02). Fluid-Structure Interaction: An Introduction to Finite Element Coupling. 1-283. https://doi.org/10.1002/9781118927762.

[25] Sun, K., Tan, J., & Wu, D. (2012, 2012/01/01/). The Research on Dynamic Rules of Crack Extension during Hydraulic Fracturing for Oil Shale In-Situ Exploitation. Procedia Environmental Sciences, 12, 736-743. https://doi.org/10.1016/j.proenv.2012.01.342.

[26] Turon, A., Camanho, P. P., Costa, J., & Dávila, C. G. (2006, 2006/11/01/). A damage model for the simulation of delamination in advanced composites under variable-mode loading. Mechanics of materials, 38(11), 1072-1089. https://doi.org/10.1016/j.mechmat.2005.10.003.

[27] Zhang, D., Wu, C., Shi, Z., Li, Y., Zhao, Y., & Wu, X. (2024). A fluid–solid coupling model for hydraulic fracture of deep coal seam based on finite element method. Physics of fluids, 36(6). https://doi.org/10. 1063/5.0213223.

[28] Zhang, G., Guo, T., Chen, M., & Qu, Z. (2025, 2025/10/01/). Investigation of hydraulic fracture initiation and propagation behavior in glutenite reservoir using an improved global cohesive zone model. Computers and Geotechnics, 186, 107421. https://doi.org/10.1016/j. compgeo. 2025. 107 421.

[29] Zhang, H.-y., Chen, J.-b., & Wang, Y. (2023, 2023/10/01). An XFEM-based CZM Numerical Strategy for Modeling Hydraulic Fracture Propagation under Different Fracturing Schemes. Journal of Physics: Conference Series, 2594(1), 012025. https://doi.org/10.1088/1742-6596/2594/1/ 0120 25.

[30] Zhou, X., Liu, X., & Liang, L. (2024). Analysis of Factors Influencing Three-Dimensional Multi-Cluster Hydraulic Fracturing Considering Interlayer Effect. Applied Sciences, 14(12), 5330. https://www. mdpi. com / 2076-3417/14/12/5330.

[31] Zhou, Y., Jia, S., Sui, Q., Wang, W., Qin, M., & Yang, D. (2025, 2025/08/01/). Investigating the impact of natural fractures on the propagation of multi-cluster fractures using XFEM. Computers and Geotechnics, 184, 107299. https://doi.org/10.1016/j.compgeo.2025.107299.

[32] Zhou, Z.-L., Hou, Z.-K., Guo, Y.-T., Zhao, H., Wang, D., Qiu, G.-Z., & Guo, W.-H. (2024, 2024/08/22/). Experimental study of hydraulic fracturing for deep shale reservoir. Engineering Fracture Mechanics, 307, 110259. https://doi.org/10.1016/j.engfracmech.2024.110259.

[33] Zhu, H., Zhao, X., Guo, J., Jin, X., An, F., Wang, Y., & Lai, X. (2015, 2015/09/01/). Coupled flow-stress-damage simulation of deviated-wellbore fracturing in hard-rock. Journal of Natural Gas Science and Engineering, 26, 711-724. https://doi.org/10.1016/j.jngse.2015.07.007.